Myocardial Perfusion: Near-automated Evaluation from Contrast-enhanced MR Images Obtained at Rest and during Vasodilator Stress[1]

Giacomo Tarroni, MS
Cristiana Corsi, PhD
Patrick F. Antkowiak, BS
Federico Veronesi, PhD
Christopher M. Kramer, MD
Frederick H. Epstein, PhD
James Walter, MD
Claudio Lamberti, MS
Roberto M. Lang, MD
Victor Mor-Avi, PhD
Amit R. Patel, MD

Purpose: To develop and validate a technique for near-automated definition of myocardial regions of interest suitable for perfusion evaluation during vasodilator stress cardiac magnetic resonance (MR) imaging.

Materials and Methods: The institutional review board approved the study protocol, and all patients provided informed consent. Image noise density distribution was used as a basis for endocardial and epicardial border detection combined with nonrigid registration. This method was tested in 42 patients undergoing contrast material–enhanced cardiac MR imaging (at 1.5 T) at rest and during vasodilator (adenosine or regadenoson) stress, including 15 subjects with normal myocardial perfusion and 27 patients referred for coronary angiography. Contrast enhancement–time curves were near–automatically generated and were used to calculate perfusion indexes. The results were compared with results of conventional manual analysis, using quantitative coronary angiography results as a reference for stenosis greater than 50%. Statistical analyses included the Student *t* test, linear regression, Bland-Altman analysis, and κ statistics.

Results: Analysis of one sequence required less than 1 minute and resulted in high-quality contrast enhancement curves both at rest and stress (mean signal-to-noise ratios, 17 ± 7 [standard deviation] and 22 ± 8, respectively), showing expected patterns of first-pass perfusion. Perfusion indexes accurately depicted stress-induced hyperemia (increased upslope, from 6.7 sec^{-1} ± 2.3 to 15.6 sec^{-1} ± 5.9; $P < .0001$). Measured segmental pixel intensities correlated highly with results of manual analysis ($r = 0.95$). The derived perfusion indexes also correlated highly with (r up to 0.94) and showed the same diagnostic accuracy as manual analysis (area under the receiver operating characteristic curve, up to 0.72 vs 0.73).

Conclusion: Despite the dynamic nature of contrast-enhanced image sequences and respiratory motion, fast near-automated detection of myocardial segments and accurate quantification of tissue contrast is feasible at rest and during vasodilator stress. This technique, shown to be as accurate as conventional manual analysis, allows detection of stress-induced perfusion abnormalities.

Supplemental material: *http://radiology.rsna.org/lookup/suppl/doi:10.1148/radiol.12112475/-/DC1*

[1] From the Department of Electronics, Computer Science and Systems, University of Bologna, Bologna, Italy (G.T., C.C., F.V., C.L.); Departments of Medicine (G.T., J.W., R.M.L., V.M., A.R.P.) and Cardiology (V.M.), University of Chicago, 5841 S Maryland Ave, MC 5084, Chicago, IL 60637; Department of Cardiology, University of Virginia, Charlottesville, Va (P.F.A., C.M.K., F.H.E.); and Department of Biomedical Engineering, University of Milan, Milan, Italy (F.V.). Received November 18, 2011; revision requested January 10, 2012; revision received January 31; accepted March 2; final version accepted April 19. **Address correspondence to** V.M. (e-mail: *vmoravi@bsd.uchicago.edu*).

Magnetic resonance (MR) imaging is increasingly used clinically to assess myocardial perfusion (1,2). Recent studies (3,4) suggest that the diagnostic accuracy of this method is comparable to or even better than that of single photon emission computed tomography (SPECT). One advantage of contrast material–enhanced cardiac MR imaging over SPECT is that it lends itself to quantitative measurement of first-pass myocardial perfusion (5–7). However, this approach relies on the definition of myocardial regions of interest (ROIs), which is usually achieved by manual tracing in one frame and then adjusting ROI position on subsequent frames to compensate for cardiac translation (8–12). This tedious, time-consuming, and subjective method has been hindering the widespread clinical application of cardiac MR imaging–based quantification of myocardial perfusion.

Advances in Knowledge

- Fast near-automated segmentation of cardiac MR images using analysis of noise distribution and spatial registration is feasible, requires less than 1 minute per image sequence, and results in myocardial regions of interest similar to those obtained by using the time-consuming multiframe manual tracing technique.
- The identified myocardial segments are suitable for semiquantitative analysis of perfusion and result in high-quality contrast enhancement curves that clearly depict expected patterns of first-pass perfusion both at rest and during vasodilator stress.
- Comparisons against invasive coronary angiography results as a reference standard showed that perfusion indexes derived from the near–automatically generated curves identified significant coronary stenoses with at least the same accuracy (sensitivity, 90%; specificity, 83%) as the manual analysis (sensitivity, 86%; specificity, 50%).

However, development of automated techniques has been difficult because of the relatively low spatial resolution and high noise levels, combined with the extreme frame-to-frame changes in both the brightness of different image components and the changing position and shape of the myocardial ROIs because of out-of-plane motion (13–15).

Recently, analysis of image noise density distribution proved a useful tool for automated dynamic detection of the left ventricular (LV) endocardial boundary throughout the cardiac cycle (16). We hypothesized that this approach could be used as a basis for near-automated definition of myocardial ROIs on first-pass perfusion cardiac MR images, a far more difficult problem to solve. Accordingly, our goal was to develop and validate a technique for near-automated definition of myocardial ROIs suitable for perfusion quantification during vasodilator stress cardiac MR imaging.

Materials and Methods

The study was funded in part by a research grant from Astellas Pharma (Deerfield, Ill), which covered regadenoson, as well as the cost of the imaging studies. The authors had full control of the data and of the information submitted for publication.

Study Design

Validation of our technique was achieved by *(a)* testing the ability to obtain contrast enhancement curves suitable for perfusion evaluation in patients undergoing vasodilator stress cardiac MR imaging and to detect stress-induced hyperemia in subjects without obstructive coronary artery disease (CAD), *(b)* comparing the near–automatically generated contrast enhancement curves and perfusion indexes against those obtained by manual tracing, *(c)* comparing the diagnostic accuracy of the near–automatically and manually derived perfusion indexes using quantitative coronary angiography results as the reference for the presence of obstructive CAD, and *(d)* comparing the accuracy of both the near-automated and manual techniques against visual interpretation. Accordingly, two separate protocols were carried out. In protocol A, to achieve goal *a*, we used contrast-enhanced cardiac MR images obtained in patients with normal perfusion. In protocol B, to achieve goals *b–d*, we used images acquired in patients suspected of having CAD who were referred for coronary angiography.

Implication for Patient Care

- The largely automated nature of our analysis combined with its high speed and high diagnostic accuracy support routine clinical use of cardiac MR imaging–based quantification of myocardial perfusion at rest and during vasodilator stress.

Population

We studied 42 patients who underwent contrast-enhanced cardiac MR imaging. These patients were selected from among 61 relevant candidates. Exclusion criteria were as follows: standard contraindications to

Published online before print
10.1148/radiol.12112475 **Content code:** CA

Radiology 2012; 265:576–583

Abbreviations:
AUC = area under the ROC curve
CAD = coronary artery disease
LV = left ventricle
ROC = receiver operating characteristic
ROI = region of interest
SNR = signal-to-noise ratio

Author contributions:
Guarantors of integrity of entire study, G.T., C.L., V.M., A.R.P.; study concepts/study design or data acquisition or data analysis/interpretation, all authors; manuscript drafting or manuscript revision for important intellectual content, all authors; manuscript final version approval, all authors; literature research, G.T., C.C., F.H.E., J.W., C.L., V.M., A.R.P.; clinical studies, C.C., C.M.K., J.W., R.M.L., V.M., A.R.P.; experimental studies, G.T., P.F.A., F.V., A.R.P.; statistical analysis, G.T., C.C., V.M., A.R.P.; and manuscript editing, G.T., C.M.K., F.H.E., J.W., C.L., R.M.L., V.M., A.R.P.

Funding:
This research was supported by the National Institutes of Health (grant UL1 RR024999).

Conflicts of interest are listed at the end of this article.

cardiac MR imaging with gadolinium enhancement, such as claustrophobia (n = 2) and implanted devices (eg, pacemakers, defibrillators) or surgical clips (a total of four patients were excluded), and contraindications to vasodilator agents, including chronic obstructive pulmonary disease (n = 3) and heart block (n = 2). Patients were also excluded if they had experienced a recent myocardial infarction (n = 5) or were older than 85 years of age (n = 3). Patients were asked to avoid β-blockers, nitrates, and caffeine before their stress cardiac MR imaging study. The institutional review boards of the University of Chicago and the University of Virginia approved the study protocol, and all patients provided informed consent.

Protocol A was performed at the University of Chicago and included 15 adult subjects (mean age, 56 years ± 15 [standard deviation]; nine men [mean age, 57 years ± 14] and six women [mean age, 54 years ± 15]; $P > .05$, Student t test) in whom CAD was ruled out by the absence of visually apparent perfusion abnormalities or late gadolinium enhancement. Protocol B was performed at the University of Virginia and included 27 patients (mean age, 64 years ± 13; 20 men [mean age, 62 years ± 12] and seven women [mean age, 65 years ± 14]; $P > .05$, Student t test) who participated in a recently reported study (9). These patients were referred for coronary angiography on the basis of abnormal SPECT findings. In these patients, coronary angiography was performed within 30 days after cardiac MR imaging.

Protocols

In protocol A, stress perfusion imaging was performed starting 1 minute after intravenous injection of the A_{2A}-specific vasodilator stress agent regadenoson (Lexiscan; Astellas Pharma [0.4-mg bolus]). Then, perfusion imaging was repeated 15 minutes after injection of aminophylline (Hospira, Lake Forest, Ill) in resting conditions. In protocol B, adenosine (Adenoscan; Astellas Pharma) was intravenously infused at a rate of 140 μg per kilogram of body weight per minute, and stress imaging was performed starting 2–3 minutes after the initiation of infusion. Resting images were obtained 10 minutes after stopping adenosine.

Cardiac MR Imaging

In each patient, short-axis images were acquired one image per cardiac cycle at three LV levels (base, middle, apex). Patients were instructed to hold their breath starting just prior to the administration of contrast material.

In protocol A, we used a 1.5-T imaging unit (Philips, Best, the Netherlands) with a phased-array cardiac coil. Images were acquired during 80–90 cardiac cycles by using a hybrid gradient-echo and echo-planar imaging sequence (17), a nonselective 90° saturation pulse followed by an 80-msec delay, a voxel size of approximately 2.5 × 2.5 mm, an acquisition time of 83 msec per section, a section thickness of 10 mm, a flip angle of 20°, a repetition time of 5.9 msec, an echo time of 2.5 msec, an echo-planar imaging factor of five, and a sensitivity factor of two. Imaging was performed during the first pass of a gadopentetate dimeglumine (Bayer Healthcare Pharmaceuticals, Wayne, NJ) bolus (0.075–0.10 mmol/kg at 4–5 mL/sec), followed by 20 mL of saline (4 mL/sec).

In protocol B, studies were performed with a 1.5-T imaging unit (Siemens Healthcare, Erlangen, Germany) with a four-channel phased-array radiofrequency coil. Imaging was performed during 40–50 cardiac cycles by using a gradient-echo and echo-planar imaging sequence, a nonselective 90° saturation pulse followed by an 80-msec delay, a field of view of 340–400 × 212–360 mm, a matrix of 128 × 80, a section thickness of 8 mm, a flip angle of 25°, a repetition time of 5.6–6.2 msec, an echo time of 1.3 msec, an echo train length of four, and effective spatial resolution of approximately 2.8 × 2.8 mm with (n = 23) or without (n = 18) rate 2 parallel imaging (18). Imaging was performed twice during the first pass of two gadopentetate dimeglumine boluses: first by using a low-dose bolus of contrast material (0.0075 mmol/kg at 4 mL/sec) to measure contrast enhancement in the LV cavity (19), and then a standard dose (0.075 at 4 mL/sec) during a separate breath hold to measure intramyocardial contrast. Each bolus was followed by 20 mL of normal saline (4 mL/sec).

Near-automated Image Analysis

Images were analyzed by using custom software that performed near-automatic image segmentation and registration on the basis of changes in noise distribution patterns (details in Appendix E1, Figs E1–E3, and Movies E1–E4 [all online]).

In the quantification of contrast material dynamics, to allow analysis of regional perfusion, the myocardial ROI was defined as the area between the detected endo- and epicardial contours. After the anterior point of insertion of the right ventricular free wall into the interventricular septum was identified by the user, this ROI was automatically divided into 16 wedge-shaped segments (six basal, six midventricular, four apical), according to the American Heart Association segmentation model (Fig E4 [online], left). Then mean pixel intensity was measured in each segment over time, resulting in contrast enhancement curves throughout the image sequence (Fig E4 [online], right).

From each segmental myocardial curve obtained at both rest and stress, the following indexes were calculated: *(a)* peak-to-peak amplitude (ie, difference between the highest and lowest points, reflecting the concentration of contrast material per unit myocardial volume); *(b)* the slope of the contrast enhancement phase, reflecting the contrast material inflow rate, calculated by using linear regression analysis of the upslope portion of the curve, beginning with the point of deflection from the background and ending just before the peak (both time points selected manually); and *(c)* the product of the amplitude and the slope. In addition, each index was normalized by its respective LV cavity value

(measured in a small circular ROI placed in the basal section and multiplied by 10 to compensate for differences in doses in protocol B). Finally, stress-to-rest ratio was calculated for each index (both nonnormalized and cavity normalized) to reflect the perfusion reserve of these indexes.

Performance Testing and Detection of Hyperemia

The quality of the contrast enhancement curves was assessed in the subjects with normal perfusion (protocol A) by calculating for each segment the ratio between the amplitude of the contrast enhancement curve and the standard deviation of its plateau phase (postpeak flat part of the curve)—that is, the signal-to-noise ratio (SNR) of each curve. This was performed separately for resting and stress images (G.T, a 4th-year PhD student).

Validation against Manual Tracing

To validate the near-automated technique against manual tracing, we analyzed images obtained in the patients suspected of having CAD (protocol B). To this effect, myocardial segments were manually traced by using commercial software (Siemens Medical Solutions, Munich, Germany), resulting in segmental mean pixel intensity over time. Perfusion indexes were calculated from these curves the same way as from the near–automatically generated curves, as described above. Mean pixel intensity in each near–automatically defined and manually traced segment was compared frame-by-frame for the resting images and separately for stress images. In addition, we compared perfusion indexes derived from near–automatically and manually generated contrast enhancement curves.

Accuracy against Coronary Angiography

Diagnostic accuracy of the near-automated analysis was evaluated side-by-side with that of the manual technique by comparing both against quantitative coronary angiography. These comparisons were first done on a segment-by-segment basis (ie, by using a myocardial segment as the unit of analysis). Each myocardial segment was classified as normal or abnormal on the basis of the presence, location, and severity of stenosis detected in the relevant coronary artery. Stenosis of greater than 50% luminal narrowing was considered as evidence of significant CAD. This classification of myocardial segments was performed by a cardiologist experienced in coronary angiography (V.M., with 5 years of experience) and was used as a reference for receiver operating characteristic (ROC) analysis. For each index, the area under the ROC curve (AUC) was averaged for the 16 myocardial segments. Sensitivity and specificity against the quantitative coronary angiography reference were calculated on a patient-by-patient basis (ie, by using the patient as the unit of analysis), while requiring at least two adjacent segments in a territory of the same coronary artery to be abnormal for a patient to be considered as having abnormal results.

Accuracy against Visual Interpretation

In addition, accuracy of both the near-automated and the manual techniques was evaluated by comparing their results against visual interpretation of perfusion image sequences. Each myocardial segment was classified as normal or abnormal on the basis of the presence of visually detectable myocardial hypoenhancement immediately following peak enhancement in the LV cavity. This classification was performed by a cardiologist experienced with cardiac MR perfusion imaging (C.M.K., with 15 years of experience) and was used as a reference for ROC analysis. For each index, AUC was averaged for the 16 myocardial segments, similar to the comparisons with quantitative coronary angiography above.

Intertechnique Comparisons of Diagnostic Accuracy

Finally, the diagnostic accuracy of the near-automated and the manual techniques were compared side-by-side with the visual interpretation against the quantitative coronary angiography reference.

Statistical Analysis

To test the ability of our technique to detect the expected hyperemic effects of regadenoson, the slope and amplitude in each segment were compared between rest and stress by using two-tailed paired Student t tests. $P < .05$ was considered to indicate a significant difference. All intertechnique comparisons were performed by using linear regression analysis with Pearson correlation coefficients and Bland-Altman analysis (20), aimed at determining the magnitude of systematic error, if any (ie, the bias), and the limits of intertechnique agreement. Comparisons of diagnostic accuracy against the quantitative coronary angiography reference were performed by using κ statistics.

Results

Time required for near-automated analysis of a complete perfusion sequence (rest or stress), including the definition of myocardial ROIs and the generation of time-intensity curves, was less than 1 minute on a personal computer (ie, up to 3 minutes for the three sections), while manual tracing required at least 10 minutes and often up to 30 minutes. This analysis resulted in endo- and epicardial boundaries that were visually judged by an expert cardiologist as reasonably accurate in all image sequences (Fig E3 [online], bottom). Regional contrast enhancement curves depicted the typical pattern of first-pass perfusion (Fig E4 [online], right) in all image sequences obtained at both rest and stress.

Mean SNR was 17 ± 7 at rest and 22 ± 8 during stress, reflecting the excellent quality of the curves. As expected in subjects with normal perfusion (protocol A), during stress, the upslope phase of the curves was steeper in all myocardial segments in all patients (Fig 1), indicating faster contrast inflow as part of the normal hyperemic response. This was reflected by the higher slope, S, during stress: 15.6 sec^{-1} ± 5.9 versus 6.7 sec^{-1} ± 2.3 at rest ($P < .0001$, paired t test). In addition, the stress-induced increase in pixel intensity, or the amplitude of the curve, A, was also

Figure 1

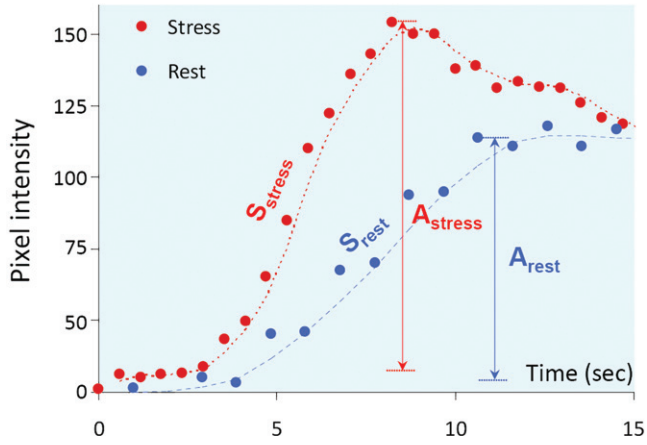

Figure 1: Graph shows example of contrast enhancement phase of the time curves obtained in the midinferior segment during rest and stress. Note the increase in both the slope *(S)* and the peak-to-peak amplitude *(A)*, reflecting the expected effects of stress. Dashed lines = spline interpolation for visualization purposes only.

higher during stress: 87 ± 25 versus 65 ± 19 ($P < .0001$), indicating increased concentration of contrast material per unit myocardial volume (Fig 1).

Of the 27 patients in protocol B, 18 had visually detectable perfusion defects during stress. Twenty-one patients had significant stenosis (defined as >50% luminal narrowing) at quantitative coronary angiography: nine (43%) had three-vessel, five (24%) had two-vessel, and seven (33%) had single-vessel disease. In these 27 patients, there were 215 segments (50%) supplied by arteries with stenosis greater than 50%, while the remaining 217 segments (50%) were supplied by arteries without significant stenosis. Figure 2 shows an example of first-pass perfusion images obtained at rest and during stress in a patient with significant stenosis. Both the near–automatically and manually generated contrast enhancement curves showed very similar patterns, depicting a stress-induced perfusion abnormality in the inferior and lateral walls.

Figure E5 (online) shows the results of the comparisons between frame-by-frame segmental pixel intensity measured automatically and that measured by using manual tracing. Excellent intertechnique agreement was noted both at rest and stress: $r = 0.95$, regression lines near unity, and virtually zero biases with reasonably narrow limits of agreement. Of note, separate analyses for basal, midventricular, and apical segments did not show any significant differences. Perfusion indexes measured by using the two techniques also showed good agreement (Table E1 [online]), as reflected by high correlations, small biases, and relatively narrow limits of agreement for most indexes (including stress amplitude, slope, and their product, both not normalized and normalized by LV cavity value and also by the corresponding resting values).

Table E2 (online) shows the summary of the ROC analysis for perfusion indexes obtained by using the near-automated and manual techniques, against both quantitative coronary angiography and visual interpretation. For both techniques, when using quantitative coronary angiography as a reference (Table E2 [online], two middle columns), the AUC varied among the calculated indexes and ranged from 0.53 to 0.73, but consistently showed highest values for the nonnormalized indexes. Importantly, for all indexes, normalized and nonnormalized (by either LV cavity or resting value or both), the AUCs were almost identical for the manual and the automated techniques. On the patient-by-patient basis, the calculated sensitivity and specificity of both techniques also varied among the calculated indexes, with the near–automatically derived stress slope showing the best diagnostic accuracy (sensitivity, 90%; and specificity, 83%), which was better than the same index obtained by manual tracing (sensitivity, 86%; and specificity, 50%). When using visual interpretation as a reference (Table E2 [online], two right columns), AUCs also varied among indexes, ranging from 0.60 to 0.78, and consistently showed highest values for cavity-normalized indexes. Similar to the comparisons with quantitative coronary angiography, AUCs were similar for the manual and the near-automated techniques.

Table E3 (online) shows the κ statistics of the comparisons against the quantitative coronary angiography reference for perfusion indexes calculated by using both near-automated and manual techniques side-by-side with the visual interpretation. While κ values were similar for the two quantitative techniques, they were higher than that for visual interpretation. Of note, the nonnormalized amplitude, slope, and their product resulted in κ values greater than 0.70, reflecting good intertechnique agreement with quantitative coronary angiography.

Discussion

This study was aimed at the development of a near-automated technique for the evaluation of myocardial perfusion from cardiac MR images, as an alternative to subjective, tedious, and time-consuming manual tracing and frame-by-frame repositioning of multiple ROIs, which is impractical for clinical use. Cardiac MR images acquired by using perfusion pulse sequences typically have relatively low spatial resolution, high noise levels, and out-of-plane cardiac motion, as well as rapid and extreme changes in brightness of the different image components. As a result, automated detection of the endo- and epicardial boundaries using conventional threshold-based approaches is not always feasible. Several previous studies (13–15,21–23) have tested

Figure 2

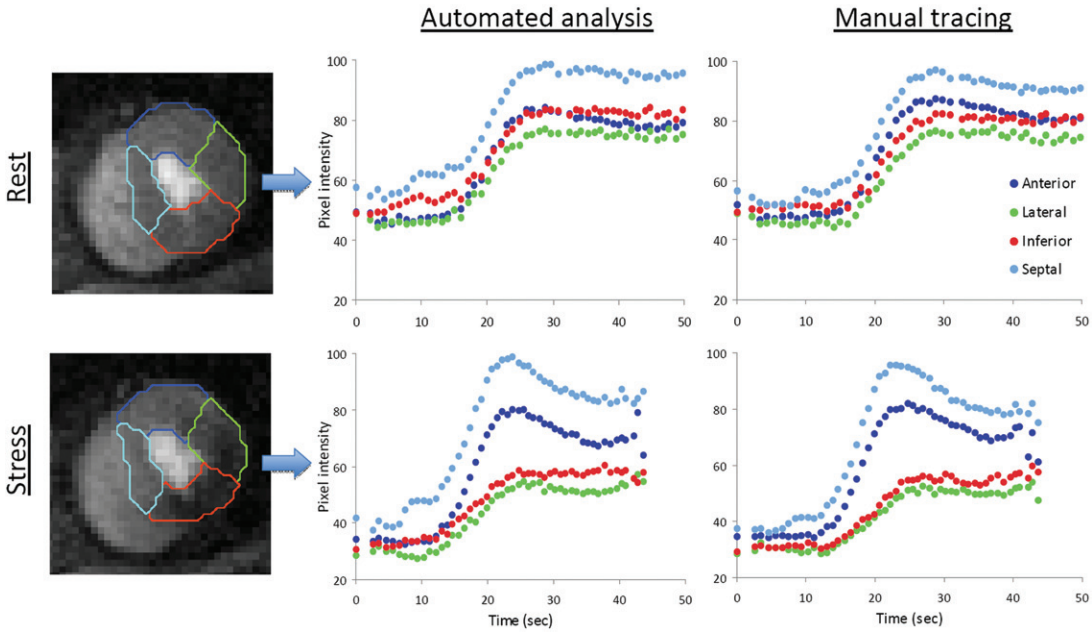

Figure 2: Example of first-pass perfusion MR images obtained at the apical LV level in a patient with stenosis greater than 50%. A stress-induced perfusion abnormality is visible in the inferior and lateral walls (bottom left). At rest, the automatically generated contrast enhancement curves (top middle) showed the same normal pattern as in Figure 1 in all four segments. With adenosine (bottom middle), both the amplitude and slope measured in the two nonaffected myocardial segments (anterior and septal) increased considerably, in contrast to the two affected segments (inferior and lateral), where these indexes were reduced. Manual tracing resulted in virtually identical curves (right).

alternative approaches to solve this problem. These studies were mostly based on either manual border initialization or thresholding of pixel intensity or required a priori knowledge of ventricular geometry to identify different anatomic components.

The novel feature of our approach is that instead it analyzes noise characteristics of the blood pool and the myocardium to differentiate between these components. To our knowledge, noise distribution–based level set techniques in combination with nonrigid multiscale registration have not been previously used to analyze contrast-enhanced cardiac MR perfusion images. The advantage of this approach is that it can depict the tissue-blood interface, irrespective of the concentration of contrast medium in the blood pool and the myocardium, even when the mean pixel intensity is almost the same. This is particularly useful for analysis of cardiac MR perfusion image sequences, in which contrast agent concentration in both image compartments goes through rapid and extreme changes from frame to frame, as the contrast agent bolus traverses the heart. Our technique was specifically designed to address this issue, and the results of this study confirmed its effectiveness. Another key difference between previously described automated techniques and our approach is that it is relatively computationally inexpensive—that is, quite fast.

This study was designed to test and validate this approach in several phases. Protocol A was aimed at testing its ability to generate time curves of myocardial intensity from image sequences acquired not only at rest but also during peak vasodilator stress. Pharmacologic stress testing is known to provide far less favorable conditions for cardiac MR imaging, because heart rates are higher and thus there is less time for imaging during the cardiac cycle. Analysis of stress images is also challenging, because breath holding with vasodilator agents is often difficult, resulting in increased cardiac translation and accentuated changes in the shape of the heart. The results of this protocol demonstrated that our technique is suitable for analysis of perfusion image sequences acquired during peak stress, as reflected by SNRs of the order of magnitude of 20. This number means that the increase in myocardial pixel intensity caused by the contrast agent bolus is 20 times the amplitude of the noise in the contrast enhancement curves, attesting to the excellent quality of these curves. In addition, we found that curves generated by using our algorithm showed the expected distinctly different patterns between rest and stress in normally perfused hearts. Analysis of these curves resulted in highly significant differences in a variety of perfusion indexes, demonstrating that these indexes are sensitive enough

to detect the normal hyperemic response to regadenoson in the absence of CAD.

Subsequently, the suitability of this near-automated approach for the diagnosis of perfusion abnormalities was tested in a group of patients with a high likelihood of CAD. To ensure that the algorithm was able to perform in a wide range of conditions, this protocol was performed at a different institution, using a different manufacturer's equipment with different settings and a different vasodilator agent. Despite these differences, our technique resulted in myocardial contrast enhancement curves that depicted the same clinical information regarding myocardial perfusion as the standard method based on manual tracing.

The perfusion indexes we studied included peak-to-peak amplitude, slope, and their product, which were previously tested by other investigators (24,25), including normalization by their corresponding values measured in the LV cavity, as well as the ratio of stress to rest values reflecting perfusion reserve. These indexes showed high levels of agreement between the near-automated and manual techniques, indicating that the former could be a useful alternative.

The final step of validation of our technique was the side-by-side comparison of its diagnostic accuracy with the manual technique against a quantitative coronary angiography reference for the presence of obstructive CAD. While the diagnostic accuracy of the slope was very good, one might argue that the AUCs of some of the other indexes obtained by either of the two techniques were not very high. This is not surprising for two reasons. First, it is well established that one cannot expect perfect agreement between the severity of coronary lesions, as determined at angiography, and their manifestation in terms of perfusion (26). Second, the ROC analysis was performed on a segment-by-segment basis, which involves a certain level of uncertainty regarding the correspondence between coronary territories and myocardial segments. Segment-by-segment or even territory-by-territory analysis of diagnostic accuracy does not usually yield high levels of accuracy, even for well-established techniques such as nuclear myocardial perfusion imaging (27). Although the true clinical value of a diagnostic technique should be tested on a patient-by-patient basis, the cohort studied in this protocol was not well suited for this goal. This is because all the patients were referred for cardiac catheterization on the basis of abnormal nuclear cardiology findings (ie, the group was biased in terms of high prevalence of disease). Importantly, however, in this cohort, the accuracy of most indexes for the detection of perfusion abnormalities was almost identical for the near-automated and the manual techniques, irrespective of the time and effort spent to analyze the image sequences. Finally, the quantitative techniques, either manual or automated, have shown better levels of agreement with quantitative coronary angiography than has visual interpretation, once again highlighting the importance of quantification.

There were limitations to our study. We referred to the analysis technique as "near-automated," as opposed to "fully automated," because it only requires manual placement of a seed point inside the LV cavity in a single frame and identification of an anatomic landmark necessary for myocardial segmentation. This level of user interaction is truly negligible compared with the current state-of-the-art technique. From our experience, this minimal input results in virtually no intermeasurement variability, which is the reason we did not include reproducibility testing in this study. Also, one might criticize our patient cohort in protocol B for the aforementioned referral bias. However, the goal of this study was not to validate the accuracy of perfusion stress cardiac MR imaging but rather to compare the performance of the newly developed near-automated technique with that of the conventional manual method.

In conclusion, this study demonstrated that despite the extreme dynamic nature of contrast-enhanced cardiac MR image sequences and respiratory motion, near-automated frame-by-frame detection of myocardial segments and high-quality quantification of myocardial contrast is feasible both at rest and during vasodilator stress. Furthermore, we found high levels of agreement between near–automatically and manually obtained perfusion indexes, as well as similar diagnostic accuracy against a quantitative coronary angiography reference. In summary, our technique provides a fast, near-automated, and user-friendly alternative to the prevailing manual method for measurement of myocardial contrast enhancement, which has been delaying the dissemination of quantitative evaluation of myocardial perfusion from cardiac MR images.

Disclosures of Conflicts of Interest: G.T. No relevant conflicts of interest to disclose. **C.C.** No relevant conflicts of interest to disclose. **P.F.A.** No relevant conflicts of interest to disclose. **F.V.** No relevant conflicts of interest to disclose. **C.M.K.** Financial activities related to the present article: none to disclose. Financial activities not related to the present article: institution has received research equipment support from Siemens Healthcare. Other relationships: none to disclose. **F.H.E.** Financial activities related to the present article: institution has received grant from Siemens Medical Solutions. Financial activities not related to the present article: none to disclose. Other relationships: none to disclose. **J.W.** No relevant conflicts of interest to disclose. **C.L.** No relevant conflicts of interest to disclose. **R.M.L.** No relevant conflicts of interest to disclose. **V.M.** No relevant conflicts of interest to disclose. **A.R.P.** Financial activities related to the present article: institution has received research grant from Astellas Pharma. Financial activities not related to the present article: none to disclose. Other relationships: none to disclose.

References

1. Klem I, Heitner JF, Shah DJ, et al. Improved detection of coronary artery disease by stress perfusion cardiovascular magnetic resonance with the use of delayed enhancement infarction imaging. J Am Coll Cardiol 2006;47(8):1630–1638.
2. Nandalur KR, Dwamena BA, Choudhri AF, Nandalur MR, Carlos RC. Diagnostic performance of stress cardiac magnetic resonance imaging in the detection of coronary artery disease: a meta-analysis. J Am Coll Cardiol 2007;50(14):1343–1353.
3. Schwitter J, Wacker CM, van Rossum AC, et al. MR-IMPACT: comparison of perfusion-cardiac magnetic resonance with single-photon emission computed tomography for the

detection of coronary artery disease in a multicentre, multivendor, randomized trial. Eur Heart J 2008;29(4):480–489.

4. Greenwood JP, Maredia N, Younger JF, et al. Cardiovascular magnetic resonance and single-photon emission computed tomography for diagnosis of coronary heart disease (CE-MARC): a prospective trial. Lancet 2012;379(9814):453–460.
5. Jerosch-Herold M, Wilke N, Stillman AE. Magnetic resonance quantification of the myocardial perfusion reserve with a Fermi function model for constrained deconvolution. Med Phys 1998;25(1):73–84.
6. Al-Saadi N, Nagel E, Gross M, et al. Improvement of myocardial perfusion reserve early after coronary intervention: assessment with cardiac magnetic resonance imaging. J Am Coll Cardiol 2000;36(5):1557–1564.
7. Rieber J, Huber A, Erhard I, et al. Cardiac magnetic resonance perfusion imaging for the functional assessment of coronary artery disease: a comparison with coronary angiography and fractional flow reserve. Eur Heart J 2006;27(12):1465–1471.
8. Fritz-Hansen T, Hove JD, Kofoed KF, Kelbaek H, Larsson HB. Quantification of MRI measured myocardial perfusion reserve in healthy humans: a comparison with positron emission tomography. J Magn Reson Imaging 2008;27(4):818–824.
9. Patel AR, Antkowiak PF, Nandalur KR, et al. Assessment of advanced coronary artery disease: advantages of quantitative cardiac magnetic resonance perfusion analysis. J Am Coll Cardiol 2010;56(7):561–569.
10. Pack NA, DiBella EV. Comparison of myocardial perfusion estimates from dynamic contrast-enhanced magnetic resonance imaging with four quantitative analysis methods. Magn Reson Med 2010;64(1):125–137.
11. McCommis KS, Goldstein TA, Abendschein DR, et al. Quantification of regional myocardial oxygenation by magnetic resonance imaging: validation with positron emission tomography. Circ Cardiovasc Imaging 2010;3(1):41–46.
12. Karamitsos TD, Leccisotti L, Arnold JR, et al. Relationship between regional myocardial oxygenation and perfusion in patients with coronary artery disease: insights from cardiovascular magnetic resonance and positron emission tomography. Circ Cardiovasc Imaging 2010;3(1):32–40.
13. Adluru G, DiBella EV, Schabel MC. Model-based registration for dynamic cardiac perfusion MRI. J Magn Reson Imaging 2006;24(5):1062–1070.
14. Gupta V, Hendriks EA, Milles J, et al. Fully automatic registration and segmentation of first-pass myocardial perfusion MR image sequences. Acad Radiol 2010;17(11):1375–1385.
15. Weng AM, Ritter CO, Lotz J, Beer MJ, Hahn D, Köstler H. Automatic postprocessing for the assessment of quantitative human myocardial perfusion using MRI. Eur Radiol 2010;20(6):1356–1365.
16. Corsi C, Veronesi F, Lamberti C, et al. Automated frame-by-frame endocardial border detection from cardiac magnetic resonance images for quantitative assessment of left ventricular function: validation and clinical feasibility. J Magn Reson Imaging 2009;29(3):560–568.
17. Ding S, Wolff SD, Epstein FH. Improved coverage in dynamic contrast-enhanced cardiac MRI using interleaved gradient-echo EPI. Magn Reson Med 1998;39(4):514–519.
18. Kellman P, Epstein FH, McVeigh ER. Adaptive sensitivity encoding incorporating temporal filtering (TSENSE). Magn Reson Med 2001;45(5):846–852.
19. Christian TF, Rettmann DW, Aletras AH, et al. Absolute myocardial perfusion in canines measured by using dual-bolus first-pass MR imaging. Radiology 2004;232(3):677–684.
20. Bland JM, Altman DG. Statistical methods for assessing agreement between two methods of clinical measurement. Lancet 1986;1(8476):307–310.
21. Dornier C, Ivancevic MK, Thévenaz P, Vallée JP. Improvement in the quantification of myocardial perfusion using an automatic spline-based registration algorithm. J Magn Reson Imaging 2003;18(2):160–168.
22. Milles J, van der Geest RJ, Jerosch-Herold M, Reiber JH, Lelieveldt BP. Fully automated motion correction in first-pass myocardial perfusion MR image sequences. IEEE Trans Med Imaging 2008;27(11):1611–1621.
23. Wollny G, Ledesma-Carbayo MJ, Kellman P, Santos A. Exploiting quasiperiodicity in motion correction of free-breathing myocardial perfusion MRI. IEEE Trans Med Imaging 2010;29(8):1516–1527.
24. Ibrahim T, Nekolla SG, Schreiber K, et al. Assessment of coronary flow reserve: comparison between contrast-enhanced magnetic resonance imaging and positron emission tomography. J Am Coll Cardiol 2002;39(5):864–870.
25. Nagel E, Klein C, Paetsch I, et al. Magnetic resonance perfusion measurements for the noninvasive detection of coronary artery disease. Circulation 2003;108(4):432–437.
26. Uren NG, Melin JA, De Bruyne B, Wijns W, Baudhuin T, Camici PG. Relation between myocardial blood flow and the severity of coronary-artery stenosis. N Engl J Med 1994;330(25):1782–1788.
27. Bateman TM, Heller GV, McGhie AI, et al. Diagnostic accuracy of rest/stress ECG-gated Rb-82 myocardial perfusion PET: comparison with ECG-gated Tc-99m sestamibi SPECT. J Nucl Cardiol 2006;13(1):24–33.
28. Mumford D, Shah J. Optimal approximation by piecewise smooth functions and associated variational problems. Pure Appl Math 1989;42(5):577–585.
29. Malladi R, Sethian JA. Image processing via level set curvature flow. Proc Natl Acad Sci U S A 1995;92(15):7046–7050.
30. Sethian JA. Level set methods and fast marching methods. Cambridge, England: Cambridge University Press, 1999.